LETTER

doi:10.1038/nature10739

Nonlinear material behaviour of spider silk yields robust webs

Steven W. Cranford[1,2], Anna Tarakanova[1,2,3], Nicola M. Pugno[4] & Markus J. Buehler[1,2,5]

Natural materials are renowned for exquisite designs that optimize function, as illustrated by the elasticity of blood vessels, the toughness of bone and the protection offered by nacre[1–5]. Particularly intriguing are spider silks, with studies having explored properties ranging from their protein sequence[6] to the geometry of a web[7]. This material system[8], highly adapted to meet a spider's many needs, has superior mechanical properties[9–15]. In spite of much research into the molecular design underpinning the outstanding performance of silk fibres[1,6,10,13,16,17], and into the mechanical characteristics of web-like structures[18–21], it remains unknown how the mechanical characteristics of spider silk contribute to the integrity and performance of a spider web. Here we report web deformation experiments and simulations that identify the nonlinear response of silk threads to stress—involving softening at a yield point and substantial stiffening at large strain until failure—as being crucial to localize load-induced deformation and resulting in mechanically robust spider webs. Control simulations confirmed that a nonlinear stress response results in superior resistance to structural defects in the web compared to linear elastic or elastic–plastic (softening) material behaviour. We also show that under distributed loads, such as those exerted by wind, the stiff behaviour of silk under small deformation, before the yield point, is essential in maintaining the web's structural integrity. The superior performance of silk in webs is therefore not due merely to its exceptional ultimate strength and strain, but arises from the nonlinear response of silk threads to strain and their geometrical arrangement in a web.

Although spider silk is used by spiders for many purposes, from wrapping prey to lining retreats[22,23], here we focus on silk's structural role in aerial webs and on how silk's material properties relate to web function. The mechanical behaviour of silk, like that of other biological materials, is determined by the nature of its constituent molecules and their hierarchical assembly into fibres[13,16,17,24–26] (Supplementary Fig. 1). Spider webs themselves are characterized by a highly organized geometry that optimizes their function[7,8,18–20]. To explore the contribution of the material characteristics to web function, we developed a web model with spiral and radial threads based on the geometry commonly found in orb webs[1]. The silk material behaviour was parameterized from atomistic simulations of dragline silk from the species *Nephila clavipes* (model A)[16,17] (Fig. 1a, b) and validated against experiments[10] (Methods Summary). Properties of silk can vary across evolutionary lineages by over 100% (refs 9, 27 and 28; Supplementary Information section 1), so we avoided species-specific silk properties and instead used a representative model to reflect the characteristic nonlinear stress–strain (σ–ε) behaviour of silk found in a web. The mechanical performance of individual silk threads has been previously investigated[10,12,13], and is in agreement with our model in terms of tensile deformation behaviour.

It is rare to see a perfectly intact web—debris, attack or unstable anchorage lead to loss of threads (see inset to Fig. 1c)—but the structure usually remains functional for a spider's use. We assessed a web's ability to tolerate defects by removing web sections (silk threads) and applying a local load (Fig. 1c). Removal of up to 10% of threads, at different locations relative to the load, had little impact on the web's response; in fact, the ultimate load capacity increased by 3–10% with the introduction of defects (Fig. 1c). We observed in all cases that failure is limited to the thread to which the force is applied. Loading of a spiral thread resulted in relatively isolated web distortion (Fig. 1e), whereas loading of a radial thread (Fig. 1f) resulted in larger deformation (about 20% more deflection and about 190% increase in energy dissipation; Fig. 1d). But in both cases, failure was localized (Fig. 1e, f). A comparative study of loading radial versus spiral threads demonstrated that the web's structural performance is dominated by the properties of the stiffer and stronger radial dragline silk (with the force required to break radial threads within the web approximately 150% higher), suggesting that the spiral threads play non-structural roles (such as capturing prey).

In situ experiments on a garden spider (*Araneus diadematus*) web (Fig. 1e, f) were in qualitative agreement with the simulations: they confirmed the prediction that failure is localized when loading either a spiral or a radial thread. Complementing these findings, we used our atomistic silk model[16,17] to connect the stress states in the web (Fig. 2a, top row) with molecular deformation mechanisms in the threads (Fig. 1a). Under loading and immediately before failure, most radial threads in the structure exhibited deformation states equivalent to the yield regime (regime II in Fig. 1a), where the presence of polymer-like semi-amorphous regions permits entropic unfolding of the silk nanocomposite under relatively low stress[16,17,29]. Once unfolding is complete, the system stiffens as stress is transferred to relatively rigid β-sheet nanocrystals[17] (regimes III–IV in Fig. 1a); it finally fails, at the thread where force is applied, because the applied stress is sufficient to rupture the nanocrystals.

Simulation and experiment both indicated that localized failure is a universal characteristic of spider webs. It is unresolved whether this behaviour is unique to silk-like materials or a result of the web's architecture (that is, a property of the construction material or of the structural design). We therefore systematically compared the response of webs constructed from three different types of fibres with distinct mechanical behaviour (Fig. 2a, left panels): in addition to fibres with the atomistically derived stress–strain behaviour of dragline silk (model A), we used idealized engineered fibres that exhibited either linear elastic behaviour (model A′) or elastic–perfectly plastic behaviour that involves severe softening (plastic yield) (model A′′). In all cases, we loaded one of the radial threads and assumed that the failure stress (about 1,400 MPa) and strain (about 67%) of silk threads are constant, so that any changes in deformation behaviour (Fig. 2a, right

[1]Laboratory for Atomistic and Molecular Mechanics (LAMM), Department of Civil and Environmental Engineering, Massachusetts Institute of Technology, 77 Massachusetts Avenue, Cambridge, Massachusetts 02139, USA. [2]Center for Materials Science and Engineering, Massachusetts Institute of Technology, 77 Massachusetts Avenue, Cambridge, Massachusetts 02139, USA. [3]Department of Applied and Engineering Physics, Cornell University, Ithaca, New York 14853, USA. [4]Laboratory of Bio-Inspired Nanomechanics "Giuseppe Maria Pugno", Department of Structural Engineering and Geotechnics, Politecnico di Torino, Corso Duca degli Abruzzi 24, 10129 Torino, Italy. [5]Center for Computational Engineering, Massachusetts Institute of Technology, 77 Massachusetts Avenue, Cambridge, Massachusetts 02139, USA.

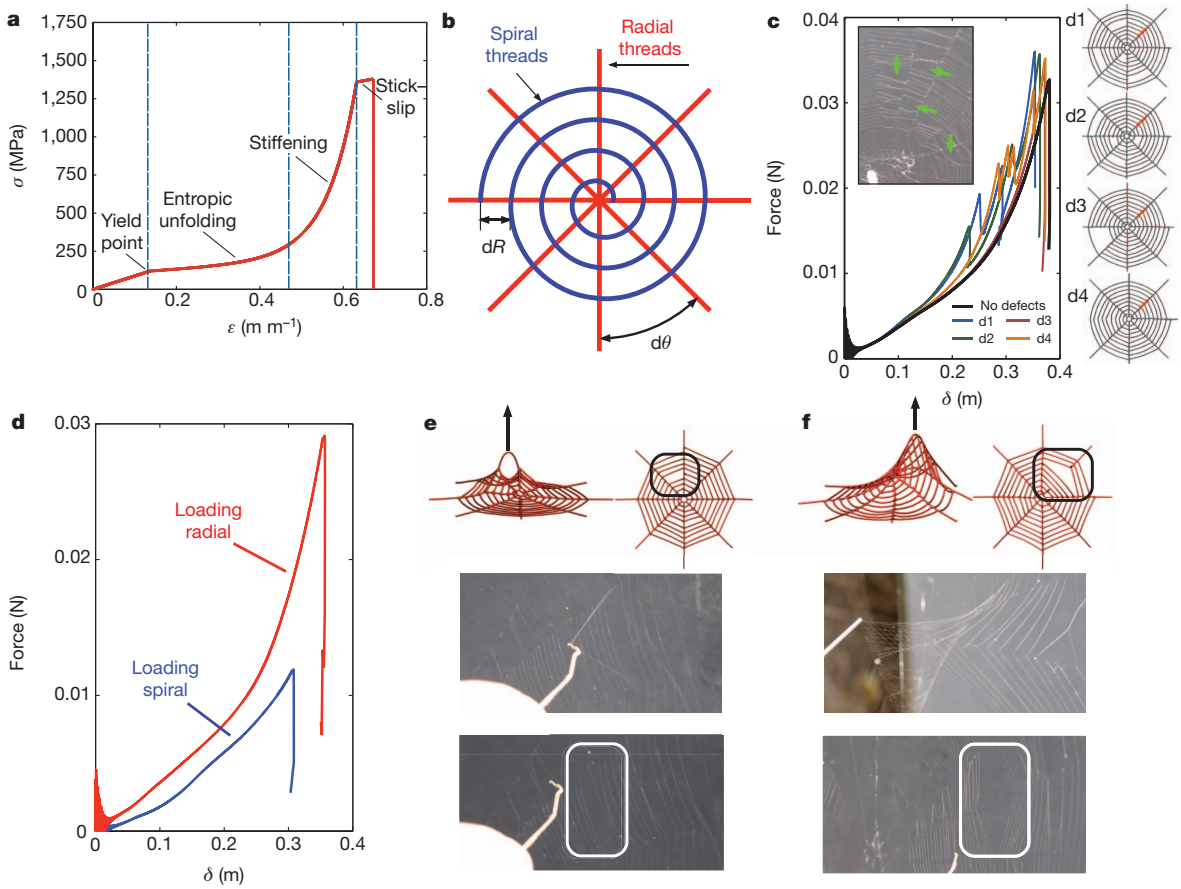

Figure 1 | Material behaviour of dragline spider silk, web model, and behaviour of webs under load. **a**, Derived stress–strain (σ–ε) behaviour of dragline silk, parameterized from atomistic simulations and validated against experiments[16,17]. There are four distinct regimes characteristic of silk[16,17]. I, stiff initial response governed by homogeneous stretching; II, entropic unfolding of semi-amorphous protein domains; III, stiffening regime as molecules align and load is transferred to the β-sheet crystals; and IV, stick–slip deformation of β-sheet crystals[16] until failure. **b**, Schematic of web model, approximated by a continuous spiral (defined by dR) supported by eight regular radial silk threads (defined by dθ), typical of orb webs[7]. **c**, Force–displacement curves for loading a defective web (results for model A; loaded region shown in red). Case studies include missing spiral segments (d1 to d3) and a missing radial thread (d4). The inset to **c** shows the *in situ* orb web as discovered, containing many defects (marked by green arrows). **d**, Force–displacement behaviour of web, comparing the loading of a single radial thread and a single spiral thread (model A). **e**, Loading of a spiral thread results in small web deformation. **f**, Loading applied at radial threads results in an increase in web deformation. In both cases (**e** and **f**) failure is isolated to the pulled thread in simulation and experiment, restricting damage to a small section of the web (indicated by white rectangles).

panels) and web damage (Fig. 2a, middle panels) would be a direct result of differences in the stress–strain behaviour of the fibres. In the case of a web comprised of natural dragline silk (top panels of Fig. 2a), all radial threads contributed partially to the resistance to loading, but the fact that the material suddenly softened at the yield point, which immediately reduced the initial modulus (about 1,000 MPa) by around 80%, ensured that only the loaded radial thread entered regime III and began to stiffen before it finally failed. With linear elastic material behaviour (middle panels of Fig. 2a), the loaded radial thread was still subjected to the bulk of the load; but adjacent radial threads bore a higher fraction of the ultimate load, which resulted in a greater delocalization of damage upon failure. With elastic–perfectly plastic behaviour (bottom panels of Fig. 2a), the softening of radial threads enhanced the load distribution even more throughout the web and thereby greatly increased the damage zone once failure occurred. The increased contribution of the auxiliary radial threads to load resistance as we moved from the natural to linear elastic to elastic–perfectly plastic behaviour resulted in 34% higher maximum strength, but 30% less displacement at failure (Fig. 2b).

The above simulations using atomistically derived silk properties (model A) assume that the spiral threads and radial threads are made of dragline silk and behave identically, except for differences arising from their different thread diameters. But in real spider webs, spiral threads are composed of more compliant and extensible viscid silk (for example, a failure strain of around 270% for the species *Araneus diadematus*[1]). To explore the effect of different silks making up the spiral and radial threads, we introduced empirically parameterized viscid spiral threads[1] (model B) and found that the results were only marginally affected (Fig. 2b). We also used a model in which we parameterized both spiral and radial threads according to empirical data[1] (model C), subjected this model to the same loading conditions and systematically compared its performance against that of models with linear elastic (model C′) and elastic–perfectly plastic behaviours (model C′′). We found similar web responses and although the web made from natural silk is weaker, it still localizes damage near the loaded region (Supplementary Information section 5).

To explore global loading responses, we subjected the web models to a homogeneously distributed wind load with effective wind speeds up to 70 m s^{-1} (a threshold at which all models fail). The system-level deflection curves (Fig. 2c) reflect the mechanical behaviour of the radial threads, which ultimately transferred load to the web's anchoring points. Although the spiral threads underwent increased deflection and captured more of the wind load owing to their larger exposed length, they were effectively pinned to the much stiffer dragline radial threads that limit web deflection (Fig. 2c, Supplementary Information section 8). For wind speeds less than 10 m s^{-1} there was little difference between the models (Fig. 2c, Supplementary Information section 8) and deflections are <12% of the total span of the web. We attributed

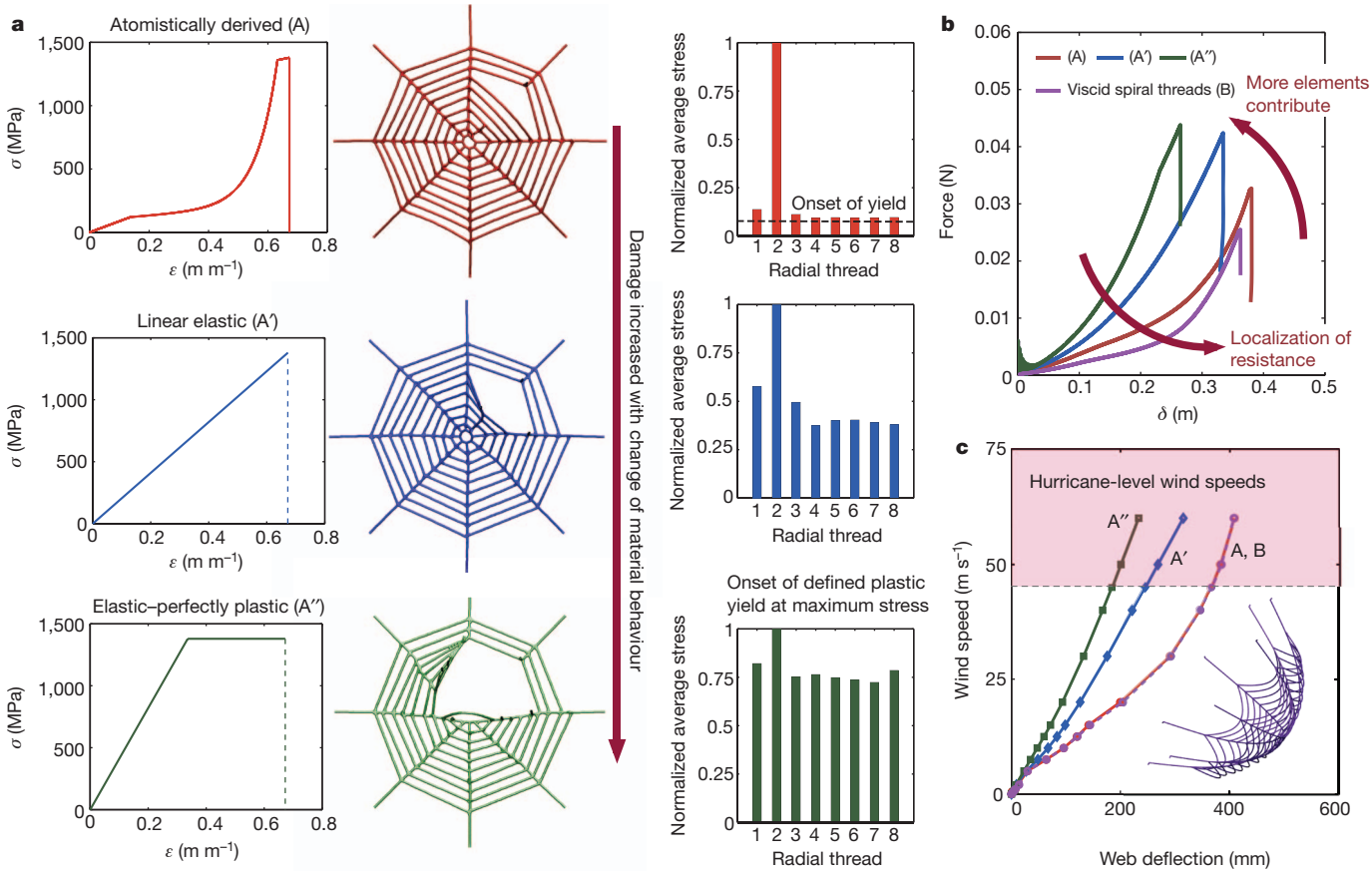

Figure 2 | Web response for varied silk behaviour under targeted (local) and distributed (global) loading. a, Comparison of failure for derived dragline silk, linear elastic and elastic–perfectly plastic behaviours (left, models A, A′ and A″). Comparison of failure (centre) confirms localized stresses and minimized damage for the natural nonlinear stiffening silk behaviour. The average stress of each radial thread (bar plots, right) reflects the nonlinear deformation states in the silk. When load is applied locally to a radial thread, other radial threads not subject to applied force reach a stress corresponding to the onset of yielding (that is, regime II in Fig. 1a). The elastic–perfectly plastic behaviour leads to an almost homogeneous distribution of stress. **b**, Force–displacement curves for varying material behaviours (models A, A′ and A″ and model B). **c**, Web behaviour under distributed (global) wind loading. The plot shows a comparison of the wind-deflection behaviour (models A, A′, A″ and B). The initial high stiffness of natural dragline silk enhances the structural integrity of the web under such loading. Failure of all webs occurs at wind speeds in excess of 60 m s^{-1}.

this relatively uniform structural rigidity of the web to the initial stiffness of the dragline silk before yield (Fig. 1a). Under higher wind loads, the softening behaviour of dragline silk at moderate deformation resulted in significant web deflection that was greater than the deflections seen with linear elastic and elastic–perfectly plastic material behaviour (Fig. 2c). We found that yield in the threads occurred at wind speeds exceeding around 5 m s^{-1}, defining a reasonable wind speed regime in which webs are operational.

Although all web models performed similarly under moderate global (wind) loading (Fig. 2c), the linear elastic and elastic–perfectly plastic models responded to targeted force application with a more catastrophic, brittle-like failure that resulted in significantly increased damage. Defining web damage as percentage of failed (broken) threads, we found that the damage of 2.5% for the natural silk behaviour increases sixfold to 15% for the elastic–perfectly plastic model (Fig. 2a, centre panel). Web performance under local loading was generalized by invoking quantized fracture mechanics[30], a theory that describes the failure mechanisms of discrete structures (such as a spider web) and adapted here to incorporate the material behaviours (Supplementary Information section 10). A generalized stress–strain behaviour, where $\sigma \propto \varepsilon^{\kappa}$ (κ is a parameter that defines the nonlinear nature of the stress–strain relationship) treated with quantized fracture mechanics revealed that the size of the damaged zone in the proximity to a defect increases for materials that feature a softening behaviour (elastic–perfectly plastic behaviour), whereas a stiffening material (natural silk) results in a decrease of the damage zone (Fig. 3). This is captured by a scaling law $\Omega(\alpha) = 1 - S^{2\alpha}$, defining the structural robustness Ω as the undamaged fraction of the web after failure. Here $\alpha = \kappa/(\kappa + 1)$ reflects the stress–strain response (linear elastic case when $\alpha = 1/2$; stiffening when α tends to 1 and softening when α tends to 0), and S is a system-dependent constant (independent of stress–strain relation). Our simulation results agreed with the predictions of quantized fracture mechanics (Supplementary Table 5) and confirmed that the relative size of the damage zone is a function of the material stress–strain relation and enhanced by the discreteness of the web (Supplementary Information section 10). This phenomenon is exemplified in spider webs (Figs 1 and 2), where the nonlinear stiffening behaviour (as α tends to 1) is essential for localizing damage and ensuring that a loaded thread becomes a sacrificial element while the majority of the web remains intact. Given the presumed metabolic effort required by the spider for rebuilding an entire web, localized failure is preferential as it does not compromise the structural integrity of the web (see Fig. 1c) and hence allows it to continue to function for prey capture in spite of the damage.

The remarkable strength, toughness and extensibility of individual spider silk threads are thus not the dominating properties that underpin the excellent structural performance of a spider web. Rather, it is the distinct nonlinear softening and subsequent stiffening of dragline silk that is essential to function, as it results in localization of damage to sacrificial threads in a web subjected to targeted (local) loading while minimizing web deformations under moderate wind (global) loading. Each regime of the nonlinear material behaviour of silk (Fig. 1a) thus

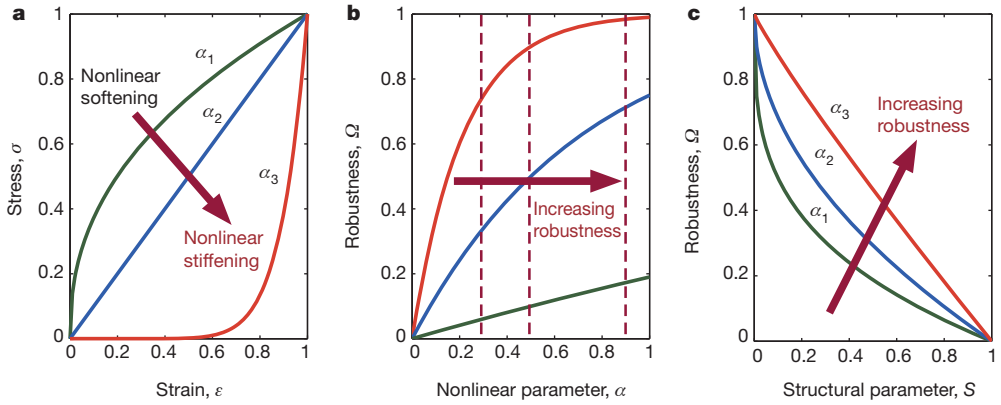

Figure 3 | Effects of stress–strain behaviour on structural robustness via quantized fracture mechanics. **a**, Plots of stress–strain curves (material behaviour) demonstrating the transition from softening to stiffening behaviours by the nonlinear parameter α ($\alpha_1 = 0.3$, $\alpha_2 = 0.5$, $\alpha_3 = 0.9$). **b**, Structural robustness Ω, defined as the undamaged fraction of the structure, versus α (dashed lines indicating α_1, α_2, α_3), given for three values of the system-dependent constant S ($S_1 = 0.1$, $S_2 = 0.5$, $S_3 = 0.9$). S captures a range of material properties (such as fracture toughness), system geometry (that is, crack width or element length), and applied loading conditions. **c**, Ω versus S. Universally, the robustness increases with an increase in α ($\alpha_1 < \alpha_2 < \alpha_3$), implying that larger nonlinear stiffening results in larger structural robustness, and hence less damage.

plays a key part in defining the overall system response in a variety of environmental settings. Other natural silk threads used to form solid materials such as cocoons, rather than aerial webs, typically display different mechanical responses[11]. Indeed, cocoon silk conforms closely to elastic–perfectly plastic behaviour, which is not suitable for web construction. The softening behaviour typically seen in such silks, combined with a solid material structure rather than a discrete mesh, results in a greater spreading of damage that effectively enhances the system's fracture toughness. This is clearly an advantage for the protective role of cocoons, and is reminiscent of other biomaterials where mechanical robustness has been attributed to the formation of large plastic regions[2,5]. The opposite is true for webs, where robustness arises from extreme localization of failure at sacrificial elements, with this behaviour enhanced by the stiffening of threads (Figs 1a and 2a).

The enhanced mechanical performance of the web relies on the integration of material and structure, which ultimately derives from the particular molecular structure of silk that features a composite of semi-amorphous protein and β-sheet nanocrystals. We suggest that web design principles might be considered in engineering, where current practice uses sacrificial elements solely to dissipate energy (for example, impact loading, seismic response). In spider webs, discrete sacrificial elements are instead a means to avoid potentially dangerous system-level loading and mitigate structural damage so that despite the small decrease in spider-web load capacity (Fig. 2b), the robustness of the structure overall is greatly enhanced (Fig. 3). This allows a spider to repair rather than rebuild completely, should failure occur. Such an engineering design could ignore the requirements for the magnitude of a potential load and allow local failure to occur, a design stipulation that requires the consideration of both material behaviour and structural architecture.

METHODS SUMMARY

The web consists of an arithmetic spiral[7] supported by radial threads at regular intervals, constructed from two primary elements, radial threads and spiral threads[7] (Fig. 1b), and is modelled using molecular dynamics procedures. We implement five material behaviours: (1) atomistically derived dragline silk behaviour (parameterized from molecular simulations of dragline silk[16,17]) (Fig. 1a); (2) empirically parameterized dragline silk (from experimental data[1]); (3) empirically parameterized viscid silk (from experimental data[1]); (4) ideal linear elastic behaviour; (5) ideal elastic–perfectly plastic behaviour, incorporated in three arrangements in models A, B and C. We consider two types of application of loading, targeted (local) and global (wind) loading. To characterize the mechanical response of the web under targeted loading, a spring-load is imposed to a small section of the web and increased until failure is incurred (defined by the failure of loaded threads). Wind loading is applied via a constant drag force applied to all web threads. *In situ* experiments through simple mechanical assays are applied to an orb web of the common European garden spider. We identify a web in its natural environment and deform radial and spiral threads using a mechanical applicator (a metal wire to load threads). During deformation we control the displacement and monitor images using a digital camera. For theoretical analysis we use quantized fracture mechanics[30], a theory that describes the failure of discrete structures such as a spider web and adapted here to incorporate the nonlinear stress–strain behaviour of silk. For a detailed description of the models see Methods and Supplementary Information.

Full Methods and any associated references are available in the online version of the paper at www.nature.com/nature.

Received 22 November 2010; accepted 25 November 2011.

1. Gosline, J. M., Guerette, P. A., Ortlepp, C. S. & Savage, K. N. The mechanical design of spider silks: from fibroin sequence to mechanical function. *J. Exp. Biol.* **202,** 3295–3303 (1999).
2. Gao, H., Ji, B., Jäger, I. L., Arzt, E. & Fratzl, P. Materials become insensitive to flaws at nanoscale: lessons from nature. *Proc. Natl Acad. Sci. USA* **100,** 5597–5600 (2003).
3. Aizenberg, J. *et al.* Skeleton of *Euplectella* sp.: structural hierarchy from the nanoscale to the macroscale. *Science* **309,** 275–278 (2005).
4. Vollrath, F. Spider webs and silks. *Sci. Am.* **266,** 70–76 (1992).
5. Kamat, S., Su, X., Ballarini, R. & Heuer, A. H. Structural basis for the fracture toughness of the shell of the conch *Strombus gigas*. *Nature* **405,** 1036–1040 (2000).
6. Lefèvre, T., Rousseau, M. E. & Pézolet, M. Protein secondary structure and orientation in silk as revealed by Raman spectromicroscopy. *Biophys. J.* **92,** 2885–2895 (2007).
7. Vollrath, F. & Mohren, W. Spiral geometry in the garden spider's orb web. *Naturwissenschaften* **72,** 666–667 (1985).
8. Vollrath, F. Silk evolution untangled. *Nature* **466,** 319 (2010).
9. Agnarsson, I., Kuntner, M. & Blackledge, T. A. Bioprospecting finds the toughest biological material: extraordinary silk from a giant riverine orb spider. *PLoS ONE* **5,** e11234 (2010).
10. Du, N. *et al.* Design of superior spider silk: from nanostructure to mechanical properties. *Biophys. J.* **91,** 4528–4535 (2006).
11. Shao, Z. Z. & Vollrath, F. Materials: surprising strength of silkworm silk. *Nature* **418,** 741 (2002).
12. Omenetto, F. G. & Kaplan, D. L. New opportunities for an ancient material. *Science* **329,** 528–531 (2010).
13. Ko, K. K. *et al.* Engineering properties of spider silk. *Adv. Fibers Plastics Laminates Composites* **702,** 17–23 (2002).
14. Rammensee, S., Slotta, U., Scheibel, T. & Bausch, A. R. Assembly mechanism of recombinant spider silk proteins. *Proc. Natl Acad. Sci. USA* **105,** 6590–6595 (2008).
15. Vollrath, F., Holtet, T., Thogersen, H. C. & Frische, S. Structural organization of spider silk. *Proc. R. Soc. Lond. B* **263,** 147–151 (1996).
16. Keten, S., Xu, Z. P., Ihle, B. & Buehler, M. J. Nanoconfinement controls stiffness, strength and mechanical toughness of beta-sheet crystals in silk. *Nature Mater.* **9,** 359–367 (2010).
17. Keten, S. & Buehler, M. J. Nanostructure and molecular mechanics of spider dragline silk protein assemblies. *J. R. Soc. Interf.* **7,** 1709–1721 (2010).
18. Aoyanagi, Y. & Okumura, K. Simple model for the mechanics of spider webs. *Phys. Rev. Lett.* **104,** 038102 (2010).
19. Ko, F. K. & Jovicic, J. Modeling of mechanical properties and structural design of spider web. *Biomacromolecules* **5,** 780–785 (2004).

20. Alam, M. S., Wahab, M. A. & Jenkins, C. H. Mechanics in naturally compliant structures. *Mech. Mater.* **39,** 145–160 (2007).
21. Alam, M. S. & Jenkins, C. H. Damage tolerance in naturally compliant structures. *Int. J. Damage Mech.* **14,** 365–384 (2005).
22. Foelix, R. F. *Biology of Spiders* 2nd edn (Oxford University Press/Georg Thieme, 1996).
23. Vollrath, F. Biology of spider silk. *Int. J. Biol. Macromol.* **24,** 81–88 (1999).
24. Termonia, Y. Molecular modeling of spider silk elasticity. *Macromolecules* **27,** 7378–7381 (1994).
25. Vepari, C. & Kaplan, D. L. Silk as a biomaterial. *Prog. Polym. Sci.* **32,** 991–1007 (2007).
26. Swanson, B. O., Blackledge, T. A. & Hayash, C. Y. Spider capture silk: performance implications of variation in an exceptional biomaterial. *J. Exp. Zool. A* **307A,** 654–666 (2007).
27. Swanson, B. O., Anderson, S. P., DiGiovine, C., Ross, R. N. & Dorsey, J. P. The evolution of complex biomaterial performance: the case of spider silk. *Integr. Comp. Biol.* **49,** 21–31 (2009).
28. Vollrath, F. & Selden, P. The role of behavior in the evolution of spiders, silks, and webs. *Annu. Rev. Ecol. Evol. Syst.* **38,** 819–846 (2007).
29. Keten, S. & Buehler, M. J. Atomistic model of the spider silk nanostructure. *Appl. Phys. Lett.* **96,** 153701 (2010).
30. Pugno, N. M. & Ruoff, R. S. Quantized fracture mechanics. *Phil. Mag.* **84,** 2829–2845 (2004).

Supplementary Information is linked to the online version of the paper at www.nature.com/nature.

Acknowledgements This work was supported primarily by the Office of Naval Research (N000141010562) with additional support from the National Science Foundation (MRSEC DMR-0819762, the NSF-REU programme, as well as CMMI-0642545) and the Army Research Office (W911NF-09-1-0541 and W911NF-10-1-0127). Support from the MIT-Italy programme (MITOR) and a Robert A. Brown Presidential Fellowship is gratefully acknowledged. N.M.P. is supported by the METREGEN grant (2009-2012) ''Metrology on a cellular and macromolecular scale for regenerative medicine''. An Ideas Starting Grant 2011 BIHSNAM on ''Bio-inspired hierarchical super nanomaterials'' was awarded to N.M.P. from the European Research Council, under the European Union's Seventh Framework Programme (FP7/2007-2013)/ERC grant (agreement number 279985). All simulations have been carried out at MIT's Laboratory for Atomistic and Molecular Mechanics (LAMM). We acknowledge assistance from S. and E. Buehler in taking photographs of the spider web.

Author Contributions S.W.C. and M.J.B. designed the research and analysed the results. S.W.C. and A.T. developed the material models, performed the simulations, and conducted the simulation data analysis. M.J.B. performed the *in situ* experiments and analysed the results. N.M.P. contributed the theoretical analysis and predictions and analysed the results. S.W.C., M.J.B., A.T. and N.M.P. wrote the paper.

Author Information Reprints and permissions information is available at www.nature.com/reprints. The authors declare no competing financial interests. Readers are welcome to comment on the online version of this article at www.nature.com/nature. Correspondence and requests for materials should be addressed to M.J.B. (mbuehler@mit.edu).

METHODS

Web geometry. Previous web models have implemented simplified versions of web geometry, most commonly in a concentric circle arrangement[18–20]. Here we modelled a realistic orb web and approximated it by an arithmetic spiral[7] defined by the polar equation $R(\theta) = \alpha \times \theta$, where spiral spacing is defined by $dR = 2\pi\alpha$, supported by radial threads at regular angular intervals ($d\theta = 45^\circ$). The basic web structure was constructed from two primary silk elements—radial threads and spiral threads[7]—combined with glue-like connections (Fig. 1b). The web was formed by particle-spring elements, with an equilibrium spacing of $r_0 = 0.01$ m. In nature, the construction of a stereotypical orb web includes the placement of framing threads that act as mooring and a structural foundation for the web[7]. The arrangement of such threads varies according to the anchoring points available to the spider and clearly has the strength necessary to bear the interior web, so we neglect it here. For a detailed description of the model, see Supplementary Information section 2.

Web models. We used web models based on combinations of five material behaviours: (1) atomistically derived dragline silk (parameterized from molecular simulations of dragline spider silk[16,17]) (Fig. 1a); (2) empirically parameterized dragline silk (from experimental data[1]); (3) empirically parameterized viscid silk (from experimental data[1]); (4) ideal linear elastic behaviour; and (5) ideal elastic–perfectly plastic behaviour. To explore the differences between the theoretically derived silk models with experimentally measured silks, the materials were implemented in the following three web models.

Model A. We used atomistically derived dragline silk behaviour for both the radial and spiral threads (details in Supplementary Information section 3.1), to maintain independence from empirical data. Even though such a simple model formulation did not allow us to draw conclusions about phenomena pertaining to specific types of silk, it did enable us to understand universal, generic relationships between underlying molecular mechanisms, the resulting nonlinear properties of the material, and the failure behaviour of webs. The dragline radial behaviour was used for fitting corresponding linear elastic (model A′, see Supplementary Information section 3.3) and elastic–perfectly plastic (model A′′, see Supplementary Information section 3.4) models, as indicated in Fig. 2a.

Model B. We combined atomistically derived dragline silk for radial threads (see Supplementary Information section 3.1) with empirically parameterized viscid silk behaviour for spiral threads (see Supplementary Information section 3.2), to examine the effect of deviations in the stiffness of viscid silk (naturally more compliant than dragline silk). Because idealized behaviours (linear elastic or elastic–perfectly plastic) are parameterized on the basis of the radial response, there are no idealized iterations of model B.

Model C. This was a completely empirically parameterized web model, with empirically fitted dragline silk for the radial threads (described in Supplementary Information section 3.2) and empirically fitted viscid silk for spiral threads, for a realistic web representation tuned by experimental data[1]. The empirical dragline behaviour is for fitting corresponding linear elastic (model C′, see Supplementary Information section 3.3) and elastic–perfectly plastic behaviour (model C′′, see Supplementary Information section 3.4).

The results of the empirically parameterized model are discussed in Supplementary Information section 5. The model framework used here can easily be adapted for other species of spiders, associated silk properties, and web geometries. Using a particle dynamics formulation (motivated by molecular dynamics), the total energy of the web system was defined as:

$$U_{\text{web}} = \Sigma_{\text{threads}} \phi_{\text{material}} \tag{1}$$

for the summation of the elastic potentials of all the silk threads, where ϕ_{material} refers to the constitutive energy expression of the specific material.

Atomistically derived dragline silk. To parameterize silk deformation behaviour, we use data from previous full atomistic simulations of major ampullate dragline spider silk[16,17,32,33], unaccounted for in previous web studies[18–20]. The constitutive behaviour of dragline silk was formulated as:

$$\varphi_{\text{dragline}}(r) = A_0 \times \begin{cases} \frac{1}{2}\frac{E_1}{r_0}(r - r_0)^2, & r \le r_y \\ \frac{r_0}{\alpha}\exp\left[\frac{\alpha(r - r_y)}{r_0}\right] + \frac{1}{2}\frac{\beta}{r_0}(r - r_y)^2 + C_1(r - r_y) + C_3, & r_y \le r < r_s \\ \frac{1}{2}\frac{E_2}{r_0}(r - r_s)^2 + C_2(r - r_s) + C_4, & r_s \le r < r_b \\ 0, & r \ge r_b \end{cases} \tag{2}$$

See Supplementary Table 1 for all parameters.

Empirically parameterized silk. To assess the generality of the results obtained with our atomistically derived behaviour, we implemented empirically fitted material behaviours for models B and C[1]. The functional form of the empirically parameterized dragline (radial) silk was identical to that of the atomistically derived dragline silk (described by equation (2)). To represent the J-shaped viscid silk response measured in experimental studies, we used a combined linear and exponential function:

$$\varphi_{\text{viscid}}(r) = A_0 \times \left(ar_0 \exp\left(\frac{r - r_0}{r}\right) + \frac{1}{2}br\frac{(r - 2r_0)}{r} + cr\right) \quad \text{for } r < r_b \tag{3}$$

We fitted the parameters in equations (2) and (3) to experiments on *Araneus diadematus*[1] for both dragline and viscid silk. See Supplementary Table 2 for all parameters.

Idealized material behaviours. For comparison, motivated by earlier studies[31], we implemented a model that allowed us systematically to vary the nature of nonlinear behaviour, permitting cases of ideal linear elastic and ideal elastic–perfectly plastic (softening) behaviour, to develop general insight. The linear elastic behaviour was governed by:

$$\varphi_{\text{linear}}(r) = \frac{1}{2}\left(\frac{E_{\text{linear}}A_0}{r_0}\right)(r - r_0)^2 \quad \text{for } r < r_b \tag{4}$$

while the elastic–perfectly plastic behaviour was governed by:

$$\varphi_{\text{plastic}}(r) = \begin{cases} \frac{E_{\text{plastic}}A_0}{2r_0}(r - r_0)^2, & r_0 \le r < r_y \\ \frac{E_{\text{plastic}}A_0}{2r_0}(r_y - r_0)^2 + \frac{E_{\text{plastic}}A_0}{r_0}(r_y - r_0)(r - r_y), & r_y \le r < r_b \end{cases} \tag{5}$$

Both behaviours were parameterized to reflect either the ultimate stress and strain of atomistically derived dragline silk (in model A) or the ultimate stress and strain of empirically parameterized dragline silk (in model C) to provide a comparison between material laws and web performance. See Supplementary Tables 3 and 4 for all parameters.

Loading conditions. We considered two types of loading, targeted (local) and global (wind) loading. To characterize the mechanical response and robustness of the web under local load, a load was imposed on a small section of the web (see Supplementary Information section 4), representing, for example, a small piece of debris. The spring-load is increased until failure occurred (defined by the failure of all loaded threads). Load was imposed on a small section of the web in the out-of-plane direction, offset from the centre of the web. Proximity to the web centre maximizes the structural resistance of the entire web (as compared to loading the web periphery, for example), while the offset is used to apply the load to a known (chosen) radial thread to ease analysis. We determined the deflection of the web (out-of-plane) and applied force. We calculated the work needed to break individual threads by numerically integrating the force–displacement curves (see Supplementary Information section 6). To characterize the mechanical response under wind load (global), we applied a constant force to the entire web structure, derived from the equivalent drag force on a cylindrical wire (see Supplementary Information section 8). Loads for equivalent wind speeds of 0.5 to 70 m s^{-1} are applied (all models fail at 70 m s^{-1} winds).

***In situ* experimental studies.** We carried out experiments on a physical web on the basis of mechanical assays applied to an orb web of the common European garden spider discovered in southern Germany. We identified a large spider web in its natural environment and ensured that the spider web was in use by a living spider. We deformed radial and spiral threads using a mechanical applicator, a small piece of wire that can effectively be used to pull on small structural features. During mechanical deformation of the web we controlled the displacement and monitored visual images of the web using a digital camera (results shown in Fig. 1e, f). A black plastic plate was placed behind the web to ensure that the web was clearly visible during the experiment for image acquisition.

Stress distribution. Normalized strain energy distributions were considered for radial threads just before and immediately after web fracture to calculate the average stress according to equations (2) to (5) (normalized with respect to maximum strain energy at ultimate failure). Spiral threads were not considered because most of the load (and thus elastic resistance) is carried by the radials in this load interval (see Supplementary Information section 9).

Theoretical analysis. We used quantized fracture mechanics[30], adapted here to incorporate the nonlinear material behaviour of silk using a generalized stress–strain (σ–ε) behaviour of $\sigma \propto \varepsilon^{\kappa}$. The relative size of the damage zone after failure was given by:

$$\varphi(\alpha) = S^{2\alpha} \tag{6}$$

where S is a system-dependent constant reflective of specific material properties (such as fracture toughness), system geometry, and applied loading conditions.

The constant S describes the damage associated with the linear elastic behaviour when 2α tends to 1 and therefore $\varphi = S$. The fraction of surviving material after failure defines structural robustness:

$$\Omega(\alpha) = 1 - S^{2\alpha} \tag{7}$$

The parameter S was determined from the linear elastic response as the reference case, and constant for all variations in the stress–strain behaviour. The three material behaviours studied here (Fig. 2a), characteristic of silk, linear elastic and elastic–perfectly plastic behaviours, were reduced to general nonlinear stress–strain power laws fitted by a single nonlinearity parameter α in the quantized fracture mechanics theory (Fig. 3). For details see Supplementary Information section 10.

31. Buehler, M. J. & Gao, H. Dynamical fracture instabilities due to local hyperelasticity at crack tips. *Nature* **439,** 307–310 (2006).
32. Nova, A., Keten, S., Pugno, N. M., Redaelli, A. & Buehler, M. J. Molecular and nanostructural mechanisms of deformation, strength and toughness of spider silk fibrils. *Nano Lett.* **10,** 2626–2634 (2010).
33. van Beek, J. D., Hess, S., Vollrath, F. & Meier, B. H. The molecular structure of spider dragline silk: folding and orientation of the protein backbone. *Proc. Natl Acad. Sci. USA* **99,** 10266–10271 (2002).